Discrete easy-axis tilting in Mn_{12}-acetate, as determined by EPR: implications for the magnetic quantum tunneling mechanism

S. Takahashi,[1] R. S. Edwards,[1] J. M. North,[2] S. Hill,[1,*] and N. S. Dalal[2]

[1]*Department of Physics, University of Florida, Gainesville, FL 32611,USA*

[2]*Department of Chemistry and National High Magnetic Field Laboratory, Tallahassee, FL 32310, USA*

(Dated: February 2, 2008)

Abstract

The variation with microwave frequency and temperature of previously reported anomalous peaks in the EPR spectra of Mn_{12}-acetate, under large transverse fields, reveals that the molecular easy magnetization axes are tilted with respect to the global symmetry direction. More importantly, on the basis of the angle-dependence of fine structures observed in the EPR spectra we infer that the tilt distribution must be discrete, as was previously suspected from studies which demonstrated the presence of a locally varying rhombic anisotropy [S. Hill *et al.*, Phys. Rev. Lett. **90**, 217204 (2003)]. The tilts are confined to two orthogonal planes, and the distribution extends up to $\sim 1.7^\circ$ degrees away from the the global easy (z-) axis. We ascribe the tilting to the hydrogen-bonding effect associated with the disordered acetic acid solvent molecules. The effect is considerably larger than deduced from x-ray diffraction analyses. These data constitute the sought-after evidence for the presence of transverse fields in Mn_{12}-acetate, and provide a possible explanation for the lack of selection rules in the resonant quantum tunneling behavior seen in low-temperature hysteresis experiments for this $S = 10$ system.

PACS numbers: 75.50.Xx, 75.60.Jk, 75.75.+a, 76.30.-v

I. INTRODUCTION

Since the discovery of magnetic quantum tunneling (MQT) in $[Mn_{12}O_{12}(CH_3COO)_{16}(H_2O)_4]\cdot\ 2CH_3COOH\cdot 4H_2O$ (Mn_{12}-ac),[1,2,3,4,5,6,7,8] single molecule magnets (SMMs) have become the focus of considerable experimental and theoretical interest due to their novel quantum properties[7,8] and possible future use in quantum computational devices.[9,10] Mn_{12}-ac remains the most widely studied SMM due to its large spin ground state ($S = 10$, see refs [5,6,7,8]), together with a considerable easy-axis magneto-crystalline anisotropy.[7,8] These combined factors result in a sizeable kinetic barrier against spin reversal at the molecular level, leading to slow magnetization relaxation and hysteresis (bistability) at low temperatures (below $\sim$3 K).[3,4] When a DC magnetic field is applied parallel to the easy-axis of a single crystal of Mn_{12}-ac, sharp steps are observed in its hysteresis loops at well defined field strengths.[5,6,7,8,11] The enhanced magnetization relaxation at these steps is the result of resonant MQT.

While a clearer picture concerning the mechanism of MQT in Mn_{12}-ac is beginning to emerge,[12,13,14,15] many interesting problems remain. In particular, current theoretical models assume the presence of quadratic and quartic transverse crystal-field interactions in the spin Hamiltonian [$\hat{O}_2^2 = \frac{1}{2}(S_+^2 + S_-^2)$ and $\hat{O}_4^4 = \frac{1}{2}(S_+^4 + S_-^4)$], where the former has been ascribed to solvent disorder.[13] However, these interactions, which contain only even powers of the raising and lowering operators, *do not* provide an explanation for the observation of 'odd' MQT steps in the hysteresis loops, i.e. tunneling via resonances between levels whose spin projections (m_s) differ by an odd integer.[7,8] It is generally recognized that the underlying mechanism *must* involve internal transverse fields,[12,16] but their source has yet to be identified. Prokof'ev and Stamp[17] proposed that hyperfine interactions might provide the answer; however, the calculated MQT rates were too small. Subsequently, Garanin and Chudnovsky[12] suggested that strains or structural defects in the crystal lattice (dislocations) could lead to a distribution of tilts of the magnetic easy-axes at the Mn_{12}-ac cluster sites; upon application of an external magnetic field, such tilts would result in a distribution of transverse fields, even when the field is applied parallel to the global symmetry (z-) axis of the crystal. While this model was in qualitative agreement with the fact that experiments revealed significant distributions in the finite field MQT rates,[18,19] the measured distributions were considerably narrower than those predicted by Garanin and Chudnovsky.[12]

Although some preliminary spectroscopic data have been reported in support of dislocations,[20] a more plausible model leading to easy-axis-tilting was recently suggested by Cornia et al.[13] Based on a detailed analysis of existing x-ray diffraction data and some approximate electronic structure calculations, they propose that such a local symmetry lowering and easy-axis-tilting can be ascribed to the presence of the two acetic acids of crystallization in the unit cell. Experiments in support of this model were recently published by us,[14] and by del Barco et al.[15] However, evidence for the easy-axis-tilting was lacking in these investigations, though we note that tilts have recently been reported for a related Mn_{12} complex in a separate study by del Barco et al.[21] Here we report electron paramagnetic resonance (EPR) measurements on precisely (in-situ) aligned Mn_{12}-ac single crystals under large applied fields in the transverse direction. At relatively low frequencies (< 90 GHz), as the field is rotated away from the hard plane, simulations show that the EPR intensity should oscillate between two series of resonances excited from "even" and "odd" spin states (labeled α and β respectively, see following section). The magnetic dipole matrix elements and transition frequencies associated with these "even" and "odd" resonances are extremely sensitive to the field orientation (providing $< 1^\circ$ resolution), allowing for a precise appraisal of the Cornia model. Indeed, experiments reveal a significant overlap of the α and β resonances, providing conclusive evidence for the presence of tilts. However, we find that the magnitude of the tilts is a factor of $4-6$ larger than predicted by Cornia et al.,[13] which should be of both theoretical and experimental significance in regards to understanding the spin dynamics of Mn_{12}-ac. Our conclusions also provide an explanation for several previously reported anomalous EPR transitions (labeled β-resonances) which cannot be explained within the widely accepted giant spin ($S = 10$) model described below.[22]

We emphasize from the outset that our conclusions are based upon the angle-dependent behavior of EPR fine structures which have previously been explained[14] within the context of the Cornia solvent-disorder picture,[13] and have been independently supported by magnetization measurements.[15] The easy axis tilting is inferred from the persistence of EPR peaks for field orientations which are tilted significantly away from the angles where the intensity should have vanished if all molecules were aligned. The discrete nature of the tilting can then be seen from the fact that the different fine structures exhibit distinct angle dependencies. This behavior is completely reproducible in Mn_{12}-ac samples prepared by different methods and by different groups.[23,24] Furthermore, our method of analysis is not sensitive to the

intricacies associated with lineshape analyses, which could be influenced by complex many-body effects, e.g. magnetic spin-spin interactions.[25] Finally, we note that all of the unusual solvent-induced anomalies reported in this paper for Mn_{12}-ac are absent in the EPR spectra for a related high-symmetry (S_4) Mn_{12} complex $[Mn_{12}O_{12}(O_2CCH_2Br)_{16}(H_2O)_4{\cdot}4CH_2Cl_2]$ which possesses a full compliment of four CH_2Cl_2 solvent molecules per Mn_{12}.[26]

II. BACKGROUND

The basis of our experiment is illustrated in Fig. 1, which shows the spin energy level diagram for Mn_{12}-ac (Fig. 1a), based on an exact diagonalization of the standard $S = 10$ spin Hamiltonian[8,13,14,15,21,22,27,28,29] under a transverse magnetic field B, and assuming S_4 symmetry:

$$\hat{H} = D\hat{S}_z^2 + \mu_B \vec{B} \cdot \vec{g} \cdot \hat{S} + B_4^0 \hat{O}_4^0 + B_4^4 \hat{O}_4^4, \tag{1}$$

Here, S_z is the projection of the spin operator $\hat{S}$ along z, and D (< 0) is the uniaxial anisotropy parameter; the second term is the Zeeman interaction; and the remaining terms represent higher order crystal field interactions (the operators $\hat{O}_4^0$ and $\hat{O}_4^4$ have their usual meaning).[8,28] We have used acceptable parameters for the simulations in Fig. 1: $D = -0.455$ cm^{-1}, $B_4^0 = -2.0 \times 10^{-5}$ cm^{-1} and $B_4^4 = \pm 3.2 \times 10^{-5}$ cm^{-1}. We note that this parameter set yields the optimum agreement with a large body of single crystal EPR data,[14,30,31,32] including the present study, which additionally considers the effects of E-strain and easy axis tilting. At this stage, we do not explicitly include lower symmetry interactions in Eq. 1 due to disorder, e.g. second-order rhombicity, or easy-axis tilting. We begin by considering a single molecule and the effect of field-mis-alignment away from the hard plane. We then compare experimental data with simulations in order to quantify the easy-axis tilting caused by the solvent-disorder in Mn_{12}-ac. Finally, we consider the rhombic anisotropy associated with this disorder. We note that an account of the influence of the solvent-disorder-induced rhombic anisotropy $[E(S_x^2 - S_y^2)]$, and its affect on the transverse field EPR fine structure, has been presented previously by us.[14,31] In the following, we use polar coordinates to parameterize the field orientation: θ represents the angle between the applied field and the global easy (z-) axis of the single crystal; ϕ represents the azimuthal angle, i.e. the angle between the intrinsic hard four-fold (x-) B_4^4 axis and the projection of the applied field onto the hard

plane.

In the high-field limit ($g\mu_B\mathbf{B} > |D|S$), and for the standard EPR geometry (microwave field $\mathbf{H}_1 \perp\mathbf{B}$), one expects a total of 20 $\Delta m = \pm 1$ EPR transitions between the 21 ($= 2S+1$) spin-states for $S = 10$. For clarity, only a few of the lowest-lying levels are shown in Fig. 1a for the case of a magnetic field applied precisely along the medium four-fold axis of a single molecule (i.e. $\theta = 90^\circ$ and $\phi = 45^\circ$); these levels are labeled on the right-hand-side of Fig. 1a according to an $\hat{S}_x$ basis, where m_x (= integer) is the projection of the total spin along the applied field axis. The high-field EPR spectra are dominated by transitions between adjacent levels, i.e. $\Delta m_x = \pm 1$. If one follows the EPR spectra to lower fields, into a region where the Zeeman and axial terms in Eq. 1 become comparable ($g\mu_B\mathbf{B} \sim |D|S$), one finds that the transitions may be grouped into two categories: i) those between levels which evolve from $m_z = \pm i$ (i = integer) zero-field doublets, which we label α (represented by blue sticks in Fig. 1a); and ii) those between levels which evolve from adjacent zero-field doublets, which we label β (represented by red solid circles in Fig. 1a). This distinction between α and β resonances is based on a zero-field $\hat{S}_z$ basis, where m_z is the projection of the total spin along the uniaxial direction of the crystal − the levels are labeled according to this convention on the left-hand-side of Fig. 1a. Throughout the remainder of the paper, we number all transitions according to the absolute value of m_x (high-field $\hat{S}_x$ representation) associated with the level from which the transition was excited, preceded by either α or β (low-field $\hat{S}_z$ representation) in order to distinguish between the two categories of resonances. Therefore, the highest field blue stick in Fig. 1a corresponds to $\alpha 10$, while the highest field red circle corresponds to $\beta 9$.[33]

In order to set the scene, we first review the status of earlier single-crystal EPR studies. The observation most pertinent to the present work is seen in Fig. 1b, which compares various calculations of the α and β transition frequencies with actual 8 K EPR peak positions.[30,31] For these earlier experiments, data were obtained with the field applied parallel to the hard plane of a single-crystal sample to within an accuracy of $\sim 1.5^\circ$ ($\theta = 90^\circ \pm 1.5^\circ$). Within the hard plane, a crude attempt was made to align the magnetic field along the medium four-fold axis. Based on our more recent angle dependent studies on accurately aligned single crystals (section III and ref. [14]), we estimate that such an alignment was achieved to within an accuracy of approximately 10° (i.e. $\phi \sim 45^\circ \pm 10^\circ$). For the purposes of the following discussion, any mis-alignment within the hard plane is not important. In

the absence of tilting, the calculated α transition frequencies decrease smoothly to zero (thick blue curves in Fig. 1b), whereas the β transition frequencies (thick red curves in Fig. 1b) go through minima which are on the order of 90 GHz for the three highest field branches. The actual β-transition data, on the other hand, deviate significantly from these predictions, i.e. they do not exhibit a minimum frequency, but instead follow monotonic curves to the lowest frequencies investigated. The same trend has been noted for field alignment along different directions within the hard plane.[30,31,32] For comparison, Fig. 2 displays representative experimental EPR spectra obtained with the field approximately along the hard four-fold axis ($\sim \phi = 0°$), also within $\pm 1.5°$ of the hard/medium plane ($\theta = 90° \pm 1.5°$);[32] note that the β-resonances are again seen to the lowest frequencies studied (44 GHz).

Following our more recent angle-dependent studies that provided clear indications for a breakdown of the four-fold symmetry of Mn_{12}-ac,[14] and in light of the Cornia model,[13] we conjecture that the anomalous behavior of the β transitions might be explained in terms of tilts of the easy-axes of magnetization at a local scale. To better illustrate this idea, we have included tilted field calculations in Fig. 1b (thin curves: blue$-\alpha$, red$-\beta$) for a few of the highest field transitions. Each tilted field curve belongs to a family of curves which deviate successively (in 0.5° increments) from one of the zero-tilt curves ($\theta = 90°$, thick lines); the tilted field curves have been truncated at low fields in order to simplify the figure. Tilting the field away from the hard plane results in a field component parallel to the easy axis. This "longitudinal" field ($B_\parallel$) has the effect of lifting the degeneracy of the of the $m_z = \pm i$ zero-field doublets in zeroth order.[34] Consequently, instead of tending to zero-frequency, the α resonance frequencies tend to successively larger offsets as the field is tilted away from the hard plane, as seen by the thin blue curves and indicated by the blue arrow (for $\alpha 10$) in Fig. 1b. The opposite is true for the β transitions. Since the longitudinal field splits the low-field $m_z = \pm i$ doublets, this results in a reduction in the closest approach of levels in adjacent doublets − hence, to a reduction in the minimum frequency of the β transitions; again, this behavior is born out by the thin red curves and indicated by the red arrow (for $\beta 9$) in Fig. 1b. Thus, tilting could explain the continuation of the β resonance data to frequencies well below the theoretical minima given by the thick red curves ($\theta = 90°$, or $B_\parallel = 0$) in Fig. 1b. However, the observed trend cannot be ascribed to a simple mis-alignment of the sample, because the $\alpha 10$ (highest field blue squares) and

$\beta 9$ (highest field red circles) resonances are both seen to frequencies below 50 GHz (see also Fig. 2). The observation of $\beta 9$ at 45 GHz would imply a sample mis-alignment of $2-3^{\circ}$, which is completely incompatible with the observed behavior of the $\alpha 10$ data which tracks the thick blue curve ($\theta = 90^{\circ}$, or $B_{\|} = 0$) in Fig. 1b; note that each successive thin curve corresponds to an additional 0.5° of tilt away from the hard plane. Thus, it would appear that the data in Figs. 1 and 2 reflect several molecular orientations.

A rigorous comparison between experiment and Eq. 1, in this frequency/field range where the Zeeman and axial terms are comparable, requires calculation of magnetic dipole matrix elements, i.e. a full simulation of the EPR spectra. Figs. 3 and 4 show 15 K EPR simulations, as a function of the polar angle θ between the applied field and the easy axis of a single molecule, and for two of the lowest frequencies used in our experiments (44 GHz and 62 GHz); the simulations are limited to the $\theta = 80^{\circ}$ to 90° range in 0.2° increments. In Figs 3a and 4a, the vertical scale represents microwave absorption while, in Figs 3b and 4b, absorption is indicated by the darker shaded regions. The simulations were generated using the software package SIM;[35,36] no rhombic (E) term was included at this stage, and the simulations assume perfect alignment of all molecules in the sample, i.e. no orientational averaging was employed. As expected, the simulations confirm that only the α peaks are observed for fields parallel to the hard plane ($\theta = 90^{\circ}$), for $f < 90$ GHz. However, tilting the field away from the hard plane leads to a very abrupt suppression of the magnetic dipole matrix elements (EPR selection rules) for the α transitions − this behavior was not obvious from Fig. 1. In just 1° of rotation, $\alpha 10$ vanishes completely at 44 GHz ($\sim 1.5^{\circ}$ for 62 GHz). This is then followed by a range of almost 2° where neither $\alpha 10$ nor $\beta 9$ are observed at the lowest frequency of 44 GHz, i.e. $\beta 9$ does not appear until the field is tilted about 2.8° away from the hard plane. Similar trends are seen at both frequencies for $\alpha 8$ and $\beta 7$, etc.., albeit over differing angle ranges. Remarkably, the simulations are suggestive of a symmetry effect in the transverse-field ($B_{\perp}$) EPR spectra, as a function of the longitudinal field component ($B_{\|} < B_{\perp}$). The dashed curves on the contour plots in Figs. 3b and 4b indicate lines of constant $B_{\|}$, demonstrating that all of the α resonances disappear (and all of the β resonances appear) at roughly the same longitudinal field strengths. Subsequently, the β resonances disappear and the α' resonances re-appear. This behavior is reminiscent of the tunnel-splittings seen in the Fe_8 SMM as a function of transverse field, for different static longitudinal fields.[37] Indeed, closer inspection of Fig. 1b reveals that the β transition frequencies tend to zero at certain

values of $B_{\|}$, while the simulations in Figs. 3 and 4 suggest that the β transitions matrix elements tend to zero as well at these same angles. Thus, the analogy with the quenching of the ground-state tunnel splittings in Fe_8 is significant, albeit the degeneracies involve excited levels evolving from different zero-field doublets in the present case. We shall not pursue this analogy further here. However, we note that the β series of resonances is exactly what one would expect from a spin $S = 9$ system in a perpendicular field with the same Hamiltonian parameters as the parent $S = 10$ system;[26,30,38] meanwhile $\alpha 8'$ corresponds to the first expected peak in a series belonging to a spin $S = 8$ system, and so on. Furthermore, all resonances except for $\alpha 10$ occur from excited levels. Thus, the tilted field data have the appearance of spectra from excited multiplets having successively lower total spin, as was originally proposed by us as an explanation for the anomalous β resonances.[30]

An intensity analysis of the measured low-frequency (< 90 GHz) $\beta 9$ peaks in Fig. 2 yields an (approximate) activation energy consistent with an excitation from the $m_x = -9$ state within the $S = 10$ manifold. We should point out that, in order to precisely fit the $\beta 9$ intensity, one must first fully comprehend its origin (we save such an analysis until the end of this article). The clearest indication that $\beta 9$ likely occurs within the $S = 10$ manifold can be seen by noting that the temperature dependencies of the $\beta 9$ and $\alpha 8$ transitions in Fig. 2 are very similar, suggesting that they both involve energy levels which are close in energy. Thus, in the following sections, we *do not* consider the possibility of excitations within excited state ($S \neq 10$) manifolds. However, the simultaneous observation of $\alpha 10$ and $\beta 9$ down to a frequency of 44 GHz (Fig. 2) *is not* consistent with the simulations in Fig. 3, which assume aligned molecules. For this reason, we argue that the molecular easy-axes are not perfectly aligned, i.e. we propose a distribution of easy-axis alignments centered about the global four-fold axis of the crystal. This would result in overlapping angle dependent features (such as those in Figs. 3 and 4) from different parts of the distribution, i.e. for a given field orientation one may observe β peaks from tilted (aligned) molecules together with α peaks due to aligned (tilted) molecules. As already discussed, the origin for such a distribution can be understood in terms of solvent disorder. Indeed, the calculations by Cornia et al. predict easy-axis tilts of up to 0.5°.[13] The absence of either $\alpha 10$ or $\beta 9$ over an approximately 2° range in the simulation in Fig. 3 suggests that the tilt distribution extends at least $\pm 1^\circ$, since both $\alpha 10$ and $\beta 9$ are observed in the 44 GHz spectra (Fig. 2).

III. EXPERIMENTAL

In order to confirm the above hypothesis, we have recently carried out extremely precise angle-dependent measurements for θ rotations away from the hard plane ($\sim 0.1^\circ$). In contrast to earlier angle-dependent investigations within the hard plane (ϕ rotations),[14] which were achieved using a rotating split-pair magnet, the present study required fields exceeding those available in the split-pair. Consequently, a unique cavity was designed and constructed, enabling in-situ rotation of the sample on the end-plate of the cylindrical cavity with an angle step of 0.18°, and in fields of up to 45 tesla (at the National High Magnetic Field Laboratory). Details concerning this cavity will be published elsewhere,[39] and an account of our EPR spectrometer is published in ref. [42]. The present investigation was carried out in a standard 9 tesla superconducting solenoid at the University of Florida. The sample was positioned on the cavity end-plate so that the plane of rotation coincided approximately with one of the four large flat faces of the needle-shaped sample. Based on comparisons with magnetic measurements,[23] we believe that this plane of rotation is inclined approximately 10° with respect to a plane containing the easy-axis and one of the hard four-fold axes, i.e. we believe $\phi \sim -10^\circ$ in these investigations (see Fig. 6 below).[32] Single crystal samples of $[Mn_{12}O_{12}(CH_3COO)_{16}(H_2O)_4]\cdot 2CH_3COOH\cdot 4H_2O$ were grown using literature methods.[43] Magnetic field dependent absorption was recorded at 15 K and at a frequency of 61.9 GHz, for field orientations roughly 3.5° either side of the hard plane ($\theta = 86.5^\circ \rightarrow 93.5^\circ$), in 0.18° increments. The experimental spectra displayed in Fig. 5 are presented in several different ways in order to aid direct comparison with Fig. 4. We note that the restricted bore size of our high-field magnet forced a lower bound on the resonance frequencies possible in the specially designed rotating cylindrical cavity.[39] Thus, high-field measurements below 61.9 GHz were not possible.

Immediately apparent from Fig. 5 is the fact that the α and β peaks overlap over a substantial angle range ($\sim 2^\circ - 3^\circ$) − particularly $\alpha 10$, $\beta 9$, and $\alpha 8$ − whereas this is not the case in Fig. 4, thus providing direct confirmation for the tilt distribution. One also observes a weak $\beta 9$ peak in Fig. 5b for field alignment precisely within the hard plane ($\theta = 90^\circ$); in fact, $\beta 9$ is reduced below the 15% level for only about 0.5° either side of the hard plane, in comparison to its complete absence over a $90^\circ \pm 2^\circ$ range in Fig. 4b. All of these facts suggest that the easy axes of some of the molecules must be tilted by up to the order of ±1.5°, i.e.

substantially greater than the tilts predicted by Cornia et al.[13] Either that, or there exists a significant distribution of internal transverse fields within the sample. However, as previously discussed, this has been ruled out by previous authors.[17] Indeed, internal fields are rather weak,[40,41] and cannot explain the present observations. Even for the worst possible sample shape, depolarization effects could account for no more than a 0.2° distribution of field orientations at the applied field strengths employed in these investigations. A more subtle, yet significant, aspect of the data in Fig. 5 is the presence of shoulders on the high-field sides of most of the EPR peaks (see Fig. 5a). These shoulders have been emphasized in Fig. 5c via the 50% contour lines (this corresponds to 50% of the maximum absorption). Such shoulders have been noted previously by us,[14] and ascribed to the solvent-disorder-induced rhombic anisotropy first proposed by Cornia et al.[13] It is evident from Figs. 5a and c that the shoulder persists over a narrower angle range, when compared to the main part of the EPR absorption peaks, i.e. suppression of the shoulder relative to the main peak is quite abrupt, occurring close to $\theta = 90 \pm 1^\circ$ for $\alpha 10$. The occurrence of distinct regions in the 3D absorption plot (Fig. 5c), with distinct angle dependencies, is suggestive of a discrete form of disorder, as originally suggested in our earlier EPR investigations.[14,44] As will become apparent later in this article, the shoulder *is* attributable to a finite rhombic term. However, the angle dependence cannot be ascribed to a rhombic term alone − one must additionally consider the combined effects of easy-axis tilting and rhombicity. In doing this, one may understand the distinct angle dependence of the main peaks and the shoulders (Fig. 5) as being due to molecules tilted in distinct (orthogonal) planes.

IV. DISCUSSION

The origin of two separate angle dependencies finds a natural explanation if one assumes that the easy-axis tilting and rhombicity are connected (as predicted by Cornia), and that the tilting is confined to directions determined by the principal axes of the rhombic zero-field tensor. We now assume that two of the Mn_{12} variants originally discussed by Cornia et al. ($n = 1$ and $n = 3$)[13] have their easy axes tilted significantly, and that these tilts are confined to two orthogonal planes defined by the associated rhombic zero-field tensor and the global four-fold (z-) axis. The $n = 1$ and $n = 3$ variants comprise 50% of the total number of molecules in Cornia's model, and both species are predicted to have significant

E values (1.6×10^{-3} cm^{-1}).[13] Of this 50%, half of the molecules (25% of the total − the **A** molecules) are expected to have their hard two-fold axes aligned along a single direction within the hard plane. Then, because there exist four equivalent positions for the acetic acid of crystallization related by a four-fold rotation about z, the remaining half of the $n = 1$ and $n = 3$ species (25% of the total − the **B** molecules) will have their hard axes aligned 90° away from the hard axes of the **A** molecules, i.e. parallel to the medium two-fold axes of the **A** molecules. This situation is depicted by the polar (ϕ-) plot in the lower panel of Fig. 6. The two-fold hard axes are denoted HE, with the subscript **A** or **B** to distinguish between the two sub-sets of molecule. The orientations of these axes relative to the four-fold hard-axes (HB_4^4 at $\phi = 0°$, 90°, 180°, and 270°) is based on previous angle-dependent EPR investigations for rotations within the hard plane, where it was determined that the principal axes of the E and B_4^4 tensors were mis-aligned by 30°.[14,32] Next, we assume that the easy axis tilts are also confined along these two distinct/discrete directions, as indicated by the shaded regions in the lower panel of Fig. 6. In other words, the well defined rhombic distortion and molecular easy axis tilting are directly related. Based on the ensuing analysis, we find that molecules tilted in one of the two orthogonal planes have their HE axes perpendicular to that plane, as shown in the upper panel of Fig. 6. Thus, the **A** (**B**) molecules are tilted in a plane containing the HE_B (HE_A) axis.

It is now possible to see how one might expect two distinct angle dependencies for different parts of the EPR spectrum, i.e. the shoulders and the main peaks. The thick purple arrow along $\phi = -10°$ (and 170°) in the lower panel of Fig. 6 represents the best estimate (*vide infra*) of the plane of rotation for the EPR spectra presented in Fig. 5. This plane is inclined closer to HE_A ($\phi = -30°$ and 150°) than to HE_B ($\phi = 60°$ and 240°). Therefore, for fields close to the hard plane ($\theta = 90°$), the rhombic term ($E\hat{O}_2^2$) associated with the $n = 1$ and $n = 3$ variants will lead to different EPR peak-position-shifts for the **A** and **B** molecules, thereby enabling one to resolve their contributions to the EPR spectra for a sufficiently large E value. In our experiments, the plane of rotation is closer to the tilt-plane for the **B** molecules than for the **A** molecules ($\Delta\phi = 20°$ as opposed to 70°). Thus, the projection of the tilt distribution onto the plane of rotation is correspondingly greater for the **B** molecules than for the **A** molecules. The magnitudes of these projections scale as the *cosine* of the angle ($\Delta\phi$) between the field rotation plane and the corresponding tilt-plane. Indeed, as explained later, it is on this basis that we deduced the orientation of the plane of rotation

relative to HE_A and HE_B for the experiments presented in Fig. 5. The molecules having the greater projection of tilts onto the rotation plane will, thus, be expected to exhibit the greater spread in their associated EPR spectra away from the hard plane. In this scenario, one may attribute the shoulders on the high-field sides of the main peaks in Fig. 5 to the **A** molecules in Fig. 6, since their tilt distribution will have a narrower projection onto the rotation plane (see projections onto field rotation plane represented by blue and red dashed lines in Fig. 6). Furthermore, the fact that the rotation plane is close to the hard axes of the **A** molecules is fully consistent with the appearance of the shoulder on the high-field sides of the main peaks (assuming $E > 0$). Meanwhile, the contribution of the **B** molecules is buried within the main peak, as explained below.

Based on the geometry depicted in Fig. 6, we set out to simulate the data in Fig. 5. The discussion above concerns only 50% of the possible variants in Cornia's model,[13] i.e. the two dominant species possessing a significant E-term. Furthermore, only half of these (25% of the total) are tilted in the plane of rotation. For the sake of simplicity, we assume that the remaining 50% of the molecules (**C**) do not possess a significant E-value. This is a slight simplification of Cornia's model, since it is known that the $n = 2$ trans species (comprising 12.5% of the molecules) are predicted to have an E-value comparable to the $n = 1$ and $n = 3$ variants.[13] However, one should first recall that Cornia's calculations are approximate, and that our previous EPR studies have indicated that the magnitudes of the E-values may have been underestimated.[14] Second, introducing too many different species would result in an over-parameterization of our model. The main purpose of the following simulation is to demonstrate that one can explain essentially all aspects of the single-crystal EPR spectra for Mn_{12}-ac based on a simple model involving three just three molecular species, together with discrete easy-axis tilting, in the spirit of the original Cornia proposal. It is not our intent that this model be viewed as definitive. Fig. 7 shows three gray-scale contour plots representing the expected angle (θ-) dependent contributions to the EPR intensity for the three species **A**, **B**, and **C**; they assume the same experimental conditions as Figs. 4 and 5, i.e. T = 15 K and a frequency of 62 GHz. The simulations in Figs. 7a and b assume that the **A** and **B** molecules are tilted respectively along the HE_A and HE_B directions ($\phi = -30°$ and 60°) i.e. the orientations of the tilt planes are "discrete." Meanwhile, we assume a non-discrete distribution of the tilt angles along these two directions, which cuts-off at $\theta = 90° \pm 1.7°$, as indicated by the shaded region in the lower panel of Fig. 6. In addition,

we assume an E-value of 0.008 cm^{-1} for the **A** and **B** species. The simulation in Fig. 7c assumes no E-value. Consequently, the EPR intensity due to the **C** molecules contributes to the bulk of the central portion of the summed EPR peaks (Fig. 8). We included a small random (i.e. not confined to planes) distribution of tilts ($\pm 1^\circ$) for the **C** molecules as a means of taking into account possible variations in the zero-field parameters/orientations associated with the four Cornia variants ($n = 0$, $n = 4$, $n = 2$ cis and trans) which comprise this remaining 50% of the molecules. It is the finite E-value associated with the **A** and **B** species which enables us to resolve the discrete nature of their tilting directions. We cannot rule out similar properties for the remaining species (**C**), but their smaller E-values do not allow us to observe such discrete behavior. Thus, the choice of random tilts for the **C** molecules is quite arbitrary. Nevertheless, this distribution provides better overall qualitative agreement with the observed out-of-plane angle dependence in Fig. 5.

Agreement between experiment (Fig. 5) and the subsequent summation of the simulated spectra (Fig. 8) is rather sensitive to the precise cut-off angle of $\theta = 90^\circ \pm 1.7^\circ$ for the tilt distribution of the **A** and **B** molecules; however, it is not so sensitive to the exact shape of the distribution. For example, a discrete distribution with the **A** and **B** molecules all having precisely $\theta = 90^\circ \pm 1.7^\circ$ tilts along HE_A and HE_B reproduces many aspects of the experiments. However, such simulations contain many more fine structures which are averaged out by considering a smoother distribution such as the one employed in the Fig. 8 simulations. Once again, we stress that this parameter set should not be viewed as definitive. However, we emphasize that, in order to simulate the main qualitative trends in the data (e.g. the distinct angle dependencies of the main peaks and high-field shoulders), a discrete tilt distribution is necessary. As discussed above, the simulations are not so sensitive to the shape of the tilt distribution within each tilt plane. Thus, it is not easy to make direct comparisons with the distributions of tilts inferred by other methods.[25] However, we note that only a small subset of the molecules (25%), corresponding to half of the lowest symmetry Cornia variants,[13] are able to contribute to the anomalous EPR intensity in our experiment. Of these molecules, we can conclude that fewer than half ($\sim$ 10% of the total) are tilted by more than 1°. While comparisons between the gray-scale plots are not so sensitive to the E-value, comparisons between simulated and actual experimental spectra are extremely sensitive to E (see Fig. 10 below); the value of 0.008(2) cm^{-1} gives the best agreement with a wide body of single-crystal data collected over several years.[14,22,30,31,44] This E value is also

in excellent agreement with a recent first principles calculation by Park et al.[45]

As discussed above, the relative angle ($\Delta\phi$) between the field rotation plane and the **A** and **B** tilt-planes (HE_B and HE_A respectively) was chosen so that the EPR peaks corresponding to the **A** and **B** molecules (Figs. 7a and b) cover the same angle ranges as the high-field shoulders ($\theta \sim 90^\circ \pm 1^\circ$ for $\alpha 10$) and the central portions of the peaks ($\theta \sim 90^\circ \pm 2^\circ$ for $\alpha 10$) respectively in Fig. 5. The best agreement was obtained with the field rotation plane oriented $\Delta\phi = 20^\circ$ away from HE_A (Fig. 6). Thus, we estimate that the HE_A and HE_B axes are oriented $\mp 20^\circ$ and $\pm 70^\circ$ with respect to the sample faces, while the hard four-fold axes are roughly $\pm 10^\circ$ away (see Fig. 6), which also agrees with magnetic and structural data.[15,23] The simulated spectra obtained according to the aforementioned procedure were then normalized and summed in the ratio $\mathbf{A}$:$\mathbf{B}$:$\mathbf{C} \equiv 25\% : 25\% : 50\%$. The results of this summation are displayed in Fig. 8. Agreement with the experimental data in Fig. 5 is quite impressive. First and foremost, the simulations including tilts account for essentially all of the anomalous aspects of the data which could not be explained without tilts (Fig. 4). For example: the $\alpha 10$ and $\beta 9$ peaks overlap by about 2° between roughly $\theta = 90^\circ \pm 0.5^\circ$ and $90^\circ \pm 2.5^\circ$; the $\beta 9$ peak disappears (below the 10% level) over a roughly $\pm 0.5^\circ$ range either side of $\theta = 90^\circ$. There is also clear evidence for a shoulder on the high-field sides of the main EPR peaks, although this shoulder is more apparent in Fig. 5a than 5b. The overall widths and shapes of the resonances are also reproduced fairly well, including the broad low-field tail and the fairly abrupt decrease in intensity on the high-field sides of the peaks (a 0.1 tesla Gaussian lineshape was employed in the individual simulations in Fig. 7). We note from Fig. 5 that an extremely weak $\beta 9$ signal persists even for fields parallel to the hard plane. We were unable to reproduce this behavior in the simulations while, at the same time, maintaining good agreement with other aspects of the experimental data, e.g. the angle range of overlap between the α and β resonances. We therefore speculate that this weak remnant signal may be due to excitations within a higher lying $S = 9$ state, as previously proposed by us.[30] However, more careful temperature dependent studies will be required in order to establish the location of this excited state relative to the $S = 10$ ground state. Indeed, recent measurements on a related high symmetry Mn_{12} species (without significant easy axis tilting) have enabled precisely such an analysis.[26]

Having satisfactorily reproduced the spectra for out-of-plane rotations (Figs. 5 and 8), we consider previously published spectra obtained as a function of the field orientation ϕ

within the hard plane.[14] One of the puzzling questions concerning these earlier measurements concerned the observation of only a single satellite peak (shoulder) on the high-field side of resonances for some field orientations. The modulation of the widths of the EPR peaks was originally explained in terms of the Cornia model.[13] So why does one never see both low-field and high-field shoulders, corresponding to the positive and negative EPR line-position-shifts induced by the different signs of the rhombic term? We note that, for a field along HE_A (HE_B), one expects an upward (downward) shift in field of the absorption due to the **A** molecules, together with a downward (upward) shift due to the **B** molecules. The apparent explanation is illustrated in Fig. 9, which displays the evolution of absorption due to one of the tilted species (either **A** or **B**) as a function of the field orientation (within the hard plane) relative to the hard two-fold axis for that species; note − this is not the same as the angle ϕ. With the field along the hard two-fold axis HE ($\phi_E \equiv 0^\circ$ in Fig. 9), the resonance occurs at the highest field position, while the projected distribution of tilts onto the rotation plane is at its narrowest. Consequently, the EPR peak is narrow. Conversely, with the field along the medium two-fold axis ($\phi_E \equiv 90^\circ$ in Fig. 9), the resonance occurs at the lowest field position, and the projected distribution of tilts onto the rotation plane is at its broadest, resulting in a broader EPR peak. Conservation of the area under the peaks additionally requires that the $\phi_E = 0^\circ$ peak be more intense at its maximum than the $\phi_E = 90^\circ$ peak. The result is that the broad low-field shoulder does not quite get resolved from the main **C** peak, whereas the sharp high-field peak is resolved for several of the resonances − particularly $\alpha 10$ and $\alpha 8$. In fact, the low-field $\phi_E = 90^\circ$ peak contributes significantly to the slow decay of the $\alpha 10$ resonance on its low-field side, thus accounting for another previously unexplained feature of the Mn_{12}-ac single-crystal EPR spectra. We note that recent experiments on deuterated samples reveal shoulders on both the low and high field sides of the main resonances.[23]

Knowing the relative orientations of the principal axes associated with the E and B_4^4 tensors, we can simulate the full hard-plane angle dependence published previously,[14] as shown in Figs. 10 to 12. We note that, while the misalignment of the E and B_4^4 tensors has previously been suggested from x-ray structure measurements, the EPR studies in ref. [14] clearly illustrate that the magnetic properties of Mn_{12}-ac reflect this misalignment. Fig. 10 displays the simulated spectra as a function of the field orientation ϕ relative to one of the hard four-fold axes (HB_4^4). These spectra can be compared directly with Fig. 1 of ref. [14], albeit that the frequencies are slightly different (50 GHz in ref. [14] and 62 GHz in the present

case). The previously published spectra do not include the highest field $\alpha 10$ resonance due to the limitations of the split-pair magnet used in those investigations; one should also be careful to note the different labeling scheme used in this and earlier studies.[33] The splitting of $\alpha 8$ (highest field peak in ref. [14]) is reproduced very precisely, as are the amplitudes of the linewidths (full-width-at-half-maximum − FWHM) variations with angle, as displayed in Fig. 11 for peaks $\alpha 2$ to $\alpha 8$. Again, these are the same four linewidths plotted in Fig. 2a of ref. [14]. The maximum linewidth or splitting caused by the disorder-induced rhombic anisotropy is observed at $\phi = \pm 60^\circ$ and $\mp 30^\circ$ relative to the HB_4^4 axes (see Fig. 6), and the widths are in fair agreement with the E-value used in the present simulations. The orientations of the linewidth maxima, which correspond to the hard and medium two-fold axes (HE_A and HE_B) are, therefore, oriented at $\pm 70^\circ$ and $\mp 20^\circ$ relative to the crystal faces. The $\pm$ and $\mp$ symbols are used here to reflect the inversion symmetry of the crystal. We note that the linewidth minima are somewhat deeper in the simulation (Fig. 11), as compared to experiment.[14] This is most likely due to other sources of line broadening (D-strain, g-strain, etc..) which were not taken into consideration in our model. The main point of this simulation is to once again show that the four-fold oscillation in the linewidth/splitting is related to the E-strain, and that the model employed in this study is in complete agreement with our earlier investigations. The contour plot in Fig. 12 clearly illustrates the four-fold variation in the line positions caused by the intrinsic four-fold $B_4^4\hat{O}_4^4$ transverse anisotropy. The orientation of one the HB_4^4 axes, together with one of the HE axes, is indicated at the top of the figure, as is the orientation of the rotation plane corresponding to the data in Fig. 5. Overall, Fig. 12 is an excellent reproduction of the contour plot in Fig. 1 of ref. [14]. We remind the reader that the linewidth/shape analysis was employed in ref. [14] to estimate the rhombic E-term associated with the low-symmetry Mn_{12} variants, and is supported by independent magnetization studies.[15] Contrary to recent assertions,[25] the EPR linewidths are not used in our determination of the easy-axis tilting, which has been inferred entirely from the angle-dependent intensities of the EPR spectra.

Finally, having reproduced the full angle dependence at a single temperature of 15 K, we display in Fig. 13 a simulation of the older temperature dependent data shown in Fig. 2. We found it necessary to include a small mis-alignment (1°, or $\theta = 89^\circ$) of the field away from the hard plane in order to obtain the appropriate relative intensities of the α and β resonances, i.e. we suspect an approximately 1° mis-alignment in the original experiment

(we note that these earlier studies were performed in a cryostat which did not allow for in-situ alignment of the sample). Within the hard plane, the simulation assumes that the field was applied along the HB_4^4 axis (i.e. $\phi = 0$). Agreement between the simulations and the experiment is extremely good.

V. SUMMARY AND CONCLUSIONS

Using angle-resolved single-crystal high-frequency EPR measurements, we have clearly demonstrated that the molecular easy axes associated with the widely studied Mn_{12}-ac single-molecule magnet are tilted on a local scale. This tilting provides the much sought-after source of the transverse fields necessary to explain the observation of 'odd' resonant tunneling steps in hysteresis experiments, i.e. the tilt distribution results in a transverse internal field distribution, even when the field is applied precisely parallel to the global easy-axis of the crystal. More importantly, on the basis of the angle-dependence of fine structures observed in the EPR spectra, we infer that the tilts are constrained along orthogonal planes, i.e. there is a discrete aspect to the tilts, as was previously suspected from studies which demonstrated the presence of a locally varying rhombic anisotropy.[14,15] This behavior is completely reproducible in Mn_{12}-ac samples prepared by different methods and by different groups.[23,24] Furthermore, our analysis is insensitive to the intricacies associated with lineshape analyses, which could be influenced by complex many-body effects, e.g. magnetic spin-spin interactions.[25] Therefore, this study provides compelling support for the recent predictions by Cornia et al.,[13] who have suggested that a discrete form of disorder associated with the acetic acid of crystallization provides the dominant source of transverse anisotropy responsible for the magnetic quantum tunneling in Mn_{12}-ac. Thus, one can rule out suggestions that dislocations may be responsible for the symmetry lowering at the local scale, since one would not expect the easy axis tilting to be confined to discrete planes under such a scenario.[12]

While our data agree with many qualitative aspects of the Cornia model,[13] the magnitudes of the easy-axis tilting angles (up to 1.7°), and the rhombic anisotropy associated with the tilted molecules (E up to 0.008 cm^{-1}), are both significantly larger than the predicted values (by a factor of about 5). These results should, therefore, be of significant theoretical interest, forming a basis for more refined structure calculations such as those recently

published by Park et al.[45] We tentatively ascribe the observed tilting to the hydrogen-bonding between the two acetic acid solvent molecules per Mn_{12}-ac. This conjecture is supported by earlier observations that hydrogen bonding must be important to the magnetization dynamics in the Mn_{12} cluster because deuteration leads to a significant slowing down of the magnetization reversal dynamics as measured by high-frequency ac susceptibility.[46] We note also that all of the unusual solvent-induced anomalies reported in this paper for Mn_{12}-ac are absent in the EPR spectra for a related high-symmetry (S_4) Mn_{12} complex $[Mn_{12}O_{12}(O_2CCH_2Br)_{16}(H_2O)_4{\cdot}4CH_2Cl_2]$ which possesses a full compliment of four CH_2Cl_2 solvent molecules per Mn_{12}, and none of the low symmetry hydrogen bonding environments present in Cornia's model.[26]

VI. ACKNOWLEDGEMENTS

We thank E. del Barco, A. Kent, G. Christou, D. N. Hendrickson and W. Wernsdorfer for useful discussion. This work was supported by the NSF (DMR0103290 and DMR0239481). S. H. acknowledges Research Corporation for financial support.

VII. REFERENCES CITED

* corresponding author, Email:hill@phys.ufl.edu

[1] R. Sessoli, H.-L. Tsai, A. R. Schake, S. Wang, J. B. Vincent, K. Folting, D. Gatteschi, G. Christou and D. N. Hendrickson, J. Am. Chem. Soc. **115**, 1804 (1993)

[2] R. Sessoli, D. Gatteschi, A. Caneschi and M. Novak, Nature **365**, 141 (1993).

[3] R. Sessoli, Mol. Cryst. Liq. Cryst. **274**, 145 (1995).

[4] M. A. Novak, R. Sessoli, A. Caneschi and D. Gatteschi, J. Magn. Magn. Mater. **146**, 211 (1995).

[5] J. R. Friedman, M. P. Sarachik, J. Tejada and R. Ziolo, Phys. Rev. Lett. **76**, 3830 (1996).

[6] L. Thomas, F. Lionti, R. Ballou, D. Gatteschi, R. Sessoli and B. Barbara, Nature **383**, 145 (1996).

[7] G. Christou, D. Gatteschi, D. Hendrickson, and R. Sessoli, MRS Bulletin **25**, 66 (2000).

[8] D. Gatteschi and R. Sessoli, Angew. Chem. **42**, 268 (2003).

[9] M. N. Leuenberger and D. Loss, Nature **410**, 789 (2001).

[10] S. Hill, R. S. Edwards, N. Aliaga-Alcalde and G. Christou, Science **302**, 1015 (2003).

[11] J. A. A. J. Perenboom, J. S. Brooks, S. Hill, T. Hathaway and N. S. Dalal, Phys. Rev. B **58**, 330 (1998).

[12] E. M. Chudnovsky and D. A. Garanin, Phys. Rev. Lett. **87**, 187203 (2001).

[13] A. Cornia, R. Sessoli, L. Sorace, D. Gatteschi, A. L. Barra and C. Daiguebonne, Phys. Rev. Lett. **89**, 257201 (2002).

[14] S. Hill, R. S. Edwards, S. I. Jones, N. S. Dalal and J. M. North, Phys. Rev. Lett. **90**, 217204 (2003).

[15] E. del Barco, A. D. Kent, E. M. Rumberger, D. N. Hendrickson and G. Christou, Phys. Rev. Lett. **91**, 047203 (2003).

[16] W. Wernsdorfer, R. Sessoli and D. Gatteschi, Europhysics Letters **47**, 254 (1999).

[17] N. V. Prokof'ev and P. C. E. Stamp, Phys. Rev. Lett. **80**, 5794 (1998).

[18] K. M. Mertes, Y. Suzuki, M. P. Sarachik, Y. Paltiel, H. Shtrikman, E. Zeldov, E. Rumberger, D. N. Hendrickson and G. Christou, Phys. Rev. Lett. **87**. 227205 (2001).

[19] E. del Barco, A. D. Kent, E. M. Rumberger, D. N. Hendrickson and G. Christou, Europhysics Letters **60**, 768 (2002).

[20] R. Amigo, E. del Barco, Ll. Casas, E. Molins, J. Tejada, I. B. Rutel, B. Mommouton, N. Dalal and J. Brooks, Phys. Rev. B **65**, 172403 (2002).

[21] E. del Barco, A. D. Kent, N. E. Chakov, L. N. Zakharov, A. L. Rheingold, D. N. Hendrickson and G. Christou, Phys. Rev. B **69**, 020411(R) (2004).

[22] S. Hill, J. A. A. J. Perenboom, N. S. Dalal, T. Hathaway, T. Stalcup and J. S. Brooks, Phys. Rev. Lett. **80**, 2453 (1998).

[23] E. del Barco, A. D. Kent, S. Hill, J. M. North, N. S. Dalal, E. M. Rumberger, D. N. Hendrickson, N. Chakov, G. Christou (unpublished); also arXiv/cond-mat/0404390.

[24] S. Hill, N. E. Chakov, N. S. Dalal, G. Christou (unpublished).

[25] W. Wernsdorfer, N. E. Chakov, G. Christou, arXix/cond-mat/0405565 (unpublished).

[26] K. Petukhov, S. Hill, N. E. Chakov, G. Christou, K. Abboud, Phys. Rev. B (in-press, 2004); also arXix/cond-mat/0403435.

[27] A. L. Barra, D. Gatteschi, R. Sessoli, Phys. Rev. B **56**, 8192 (1997).

[28] I. Mirebeau, M. Hennion, H. Casalta, H. Andres, H. U. Gudel, A. V. Irodova, and A. Caneschi, Phys. Rev. Lett. **83**, 628 (1999).

[29] A. Mukhin, V. D. Travkin, A. K. Zvezdin, S. P. Lebedev, A. Caneschi, and D. Gatteschi, Europhys. Lett. **44**, 778 (1998).

[30] S. Hill, R. S. Edwards, J. M. North, S. Maccagnano and N. S. Dalal, Polyhedron **22**, 1897 (2003).

[31] S. Hill, R. S. Edwards, J. M. North, K. Park and N. S. Dalal, Polyhedron **22**, 1889 (2003).

[32] The sign of B_4^4 dictates the hard and easy directions of magnetization, which are separated by 45° from each other in the xy-plane; the hard directions are along x and y for $B_4^4 > 0$, and at 45° to x and y for $B_4^4 < 0$. In a recent investigation, we estimated that the hard axes are approximately aligned with the edges of the square cross-section of a typical Mn_{12}-ac single crystal sample, with the medium axes oriented approximately accross the diagonals. Based on more comprehensive studies, including comparisons between the present work and recent magnetic measurements,[15] we now believe that the four-fold axes are shifted approximately $10° \pm 5°$ away from the crystal faces, i.e. at 10°, 55°, 90°, 145°, etc. This does not invalidate any of the conclusions of our earlier studies, particularly the relative orientations of the E and B_4^4 tensors. A full account of the symmetries associated with the MQT in Mn_{12}-ac will be presented elsewhere.[23]

[33] We note that this numbering convention differs slightly from the scheme used in earlier publications. We previously used all integers when numbering the α and β resonances. This scheme ignores the obvious symmetries associated with the various transitions. Therefore, we now use only even integers for α resonances, and odd integers for β resonances, i.e. $\alpha 9$ under the old notation is now $\alpha 8$, $\beta 10$ is $\beta 9$, $\alpha 8$ is $\alpha 6$, and so on.[22]

[34] In contrast to $B_{\|}$, the "transverse" field ($B_{\perp}$) acts on the low-field $m_z = \pm i$ doublets only in high orders of perturbation theory (the order depends explicitly on the nature of other transverse terms in $\hat{H}$). At high fields ($g\mu_B \mathbf{B} > |D|S$), the Zeeman term operates only in zeroth order, since it defines the appropriate basis functions.

[35] Written by H. Weihe, University of Copenhagen, http://sophus.kiku.dk/software/epr/epr.html.

[36] C. J. H. Jacobsen, E. Pedersen, J. Villadsen, H. Weihe, Inorg. Chem. **32**, 1216-1221 (1993).

[37] W. Wernsdorfer and R. Sessoli, Science **284**, 133 (1999).

[38] D. Zipse, J. M. North, N. S. Dalal, S. Hill, R. S. Edwards, Phys. Rev. B **68**, 184408 (2003).

[39] S. Takahashi and S. Hill, submitted.

[40] B. Parks, J. Loomis, E. Rumberger, D. N. Hendrickson, G. Christou, Phys. Rev. B **64**, 184426 (2001).

[41] K. Park, M. A. Novotny, N. S. Dalal, S. Hill, P. A. Rikvold, Phys. Rev. B **66**, 144409 (2002).

[42] M. Mola, S. Hill, P. Goy and M. Gross, Rev. Sci. Inst. **71**, 186 (2000).

[43] T. Lis, Acta Crystallogr. **B36**, 2042 (1980).

[44] S. Hill, S. Maccagnano, K. Park, R. M. Achey, J. M. North and N. S. Dalal, Phys. Rev. B **65**, 224410 (2002).

[45] K. Park, T. Baruah, N. Bernstein, and M. R. Pederson, Phys. Rev. B **69**, 144426 (2004).

[46] R. Blinc, B. Zalar, A. Gregorovic, D. Arcon, Z. Kutnjak, C. Filipic, A. Levstik, R.M. Achey and N.S. Dalal, Phys. Rev. B **67**, 094401 (2003).

Figure captions

FIG. 1. (a) Energy level diagram for Mn_{12}-ac with the field applied in the hard plane ($\theta = 90°$, $\phi = 45°$); the crystal-field parameters used for the simulation are given in the main text. The labels on the left hand side of the figure correspond to the spin projection along z (low-field m_z basis), while the labels on the right correspond to the spin projection along the applied field direction (high-field m_x basis). The vertical blue sticks illustrate the origin of the α EPR transitions, while the filled red circles represent the high-frequency β-transitions. (b) A comparison between measured and calculated α and β EPR transition frequencies, as a function of the applied magnetic field strength. The open blue squares (α) and red circles (β) represent experimental data obtained at 8 K. The thick curves illustrate the expected behavior of the EPR transition frequencies for precise field alignment within the hard plane ($\theta = 90°$), i.e. no tilting of the molecules. Note that, for this case, the α frequencies decrease smoothly to zero as the field tends to zero, whereas the β frequencies go through a minimum ($\sim 90 - 95$ Ghz for the highest field transitions) and then tend to a finite zero-field offset. The thin curves illustrate the dependence of the α and β transition frequencies upon tilting the field away from the hard plane; each thin curve represents an additional 0.5° of tilt away from the hard plane ($\theta = 90°$), and the curves have been truncated at low fields in order to simplify the figure. The red arrow illustrates the depression of the minimum β frequency, while the blue arrow illustrates the corresponding increase in the minimum α frequency.

FIG. 2. Temperature and frequency dependence of the EPR spectra obtained with the magnetic field applied approximately parallel to the hard four-fold axis of the crystal;[30,31] the frequencies and temperatures are indicated in the figure. These experiments were performed using instrumentation that did not allow for in-situ alignment of the sample. Based on subsequent analysis, we estimate a slight ($\sim 1°$) mis-alignment of the field away from the hard plane (see also Fig. 13), i.e. $\theta = 89°$ and $\phi \sim 0°$. The data clearly demonstrate that both the α and β resonances persist to the lowest frequency (44.3 GHz), in apparent conflict with the predictions of Fig. 1, thus suggesting that a significant fraction of the molecules may be tilted with respect to the global easy axis of the crystal (see text). The γ resonance has been previously attributed to a small fraction ($< 5\%$) of Mn_{12} molecules having lower symmetry (i.e. different crystal field parameters) than the acetate.[30]

FIG. 3. Simulations of 15 K, 44 GHz, EPR spectra as a function of the field orientation θ (in 0.2° increments) relative to the easy axis of a single molecule ($\phi = 0°$). In (a) the vertical scale represents absorption (arb. units) while, in (b), absorption is indicated by the darker shaded regions. The parameters used for these simulations are given in the main text. In (b), the dashed curves represent constant values of the longitudinal field $B_{\|}$. The key point to note is the alternate appearance and disappearance of even α peaks and odd β peaks.

FIG. 4. Simulations of 15 K, 62 GHz, EPR spectra as a function of the field orientation θ (in 0.2° increments) relative to the easy axis of a single molecule ($\phi = 0°$). In (a) the vertical scale represents absorption (arb. units) while, in (b), absorption is indicated by the darker shaded regions. The parameters used for these simulations are given in the main text. In (b), the dashed curves represent constant values of the longitudinal field $B_{\|}$. The key point to note is the alternate appearance and disappearance of even α peaks and odd β peaks.

FIG. 5. a) Experimental EPR spectra obtained at 15 K and 62 GHz, as a function of the field orientation θ (in 0.18° increments) relative to the global easy (z-) axis of a single crystal sample; the red data represent $\theta = 90°$. These experiments were performed using instrumentation that *did* allow for in-situ rotation of the sample about 1 axis.[39] We estimate (see main text) that the rotation plane was 10° away from one of the hard B_4^4 axes within the hard (xy-) plane. To aid comparisons, the data in b) are plotted in the same fashion as Fig. 4a, while the data in c) are plotted in the same fashion as Fig. 4b. In (b) the vertical scale represents absorption (arb. units). In (c) absorption is indicated by the darker shaded regions; 15% and 50% (of maximum absorption) contour lines have been included to aid the discussion in the main text. No noise reduction/filtering has been applied to the data. The main points to note are the significant overlap of intensity due to the α and β resonances, and the distinct shoulders on the high field sides of the peaks which have been emphasized with the 50% contour lines.

FIG. 6. Schematic illustrating the discrete nature of the proposed tilting of various Mn_{12} species. Upper panel: illustration of the tilt distribution for the **A** molecules, wherein the tilts are confined to the plane containing the crystallographic easy (z-) axis and the hard two-fold axis of the **B** molecules ($HE_B \equiv$ medium two-fold axis of the **A** molecules); meanwhile, the hard two-fold axis of the **A** molecules (HE_A) is perpendicular to the tilt

plane; an orthogonal situation exists for the **B** molecules. Lower panel: a polar plot (θ is radial and ϕ is azimuthal) illustrating the orientations of the two tilt planes (shaded areas), and the principal axes associated with the intrinsic four-fold anisotropy ($\hat{O}_4^4$) and disorder induced two-fold anisotropies ($\hat{O}_2^2$) associated with two of the Mn_{12} variants (**A** and **B**); HE_A and HE_B refer respectively to the hard two-fold axes for the **A** and **B** molecules; HB_4^4 and MB_4^4 refer respectively to the global hard and medium four-fold axes; the purple arrow indicates the plane of rotation for the experiments shown in Fig. 5, while the red and blue dashed lines respectively indicate the extent of the projections of the tilts of the **A** and **B** molecules onto the rotation plane. Note the $\Delta\phi = 30^\circ$ offset between the $\hat{O}_4^4$ and $\hat{O}_2^2$ tensors.

FIG. 7. Simulated contributions to the angle dependent EPR spectrum for the **A**, **B** and **C** molecules, for θ rotations in a plane which is inclined $\Delta\phi = 20^\circ$ away from the tilt plane associated with the **B** molecules (70° away from the **A** tilt plane, see also Fig. 6). The temperature is 15 K and the frequency is 62 GHz; see main text for a detailed explanation of these simulations. The E-term associated with the **A** and **B** molecules splits their contribution to the spectrum. The near coincidence of the rotation plane and the hard axis of the **A** molecules shifts the contribution to the intensity to higher (lower) fields for the **A** (**B**) molecules. Meanwhile, the near coincidence of the rotation plane and the **B** tilt plane (see Fig. 6) projects almost the full tilt distribution for the **B** molecules, i.e. the absorption due to the **B** molecules extends over a wider angle range either side of the hard plane ($\theta = 90^\circ$) compared to either **A** or **C**, thus accounting for the overlapping α and β resonances in Fig. 5. In contrast, the angle dependence of the EPR spectra associated with the **A** and **C** molecules does not differ greatly from the simulation in Fig. 4 (with no tilting).

FIG. 8. a) Angle dependent 25%:25%:50% summations of the normalized spectra for the **A**, **B** and **C** molecules from Fig. 7; each successive trace corresponds to a 0.2° increment in θ, and the red trace represents $\theta = 90^\circ$. In b), the same data are displayed in a 3D gray-scale for direct comparisons with earlier figures; the 10% and 50% (of maximum absorption) contours are intended as guides to the eye. These simulations are to be compared with the experimental data in Fig. 5. In particular, the high-field shoulder is reproduced (see also Fig. 10), as well as the considerable angle overlap of the α and β resonances.

FIG. 9. Simulated evolution of absorption due to either of the tilted species (**A** or **B**) as a function of the field orientation (ϕ_E, within the hard plane) relative to the hard two-fold

axis for that species (note - this is not the same as the angle ϕ); the temperature is 15 K and the frequency is 62 GHz. With the field along the hard two-fold axis HE ($\phi_E \equiv 0°$), the resonance occurs at the highest field position, while the projected distribution of tilts onto the rotation plane is at its narrowest. Consequently, the EPR peak is narrow, forming a sharp shoulder on the high field side of the summed spectra (see Figs. 8 and 10). Conversely, with the field along the medium two-fold axis ($\phi_E \equiv 90°$), the resonance occurs at the lowest field position, and the projected distribution of tilts onto the rotation plane is at its broadest, resulting in a broader EPR peak, which contributes to the low-field tail of the summed spectra.

FIG. 10. Simulated ϕ-dependence of the 62 GHz, 15 K, EPR spectra incorporating the $\Delta\phi = 30°$ mis-alignment between the intrinsic four-fold $\hat{O}_4^4$ tensor and the disorder-induced two-fold $\hat{O}_2^2$ tensors for the **A** and **B** molecules. These data compare favorably with previously published data (see Fig. 1 of ref. [14]).

FIG. 11. Azimuthal angle (ϕ-) dependence of the full-widths-at-half-maximum (FWHM) for several of the α peaks in Fig. 10 ($\alpha 2$ to $\alpha 8$). This figure is to be compared directly with Fig. 2a of ref. [14].

FIG. 12. Grayscale contour plot corresponding to the data in Fig. 11. The black dashed line indicates the orientation corresponding to the data in Fig. 5. The orientations of one of the HE axes and one of the HB_4^4 axes are indicated at the top of the figure. This figure is to be compared directly with the contour plot Fig. 1 of ref. [14] (note the slightly different labeling used in these two figures[33]); the white dashed lines in the present figure correspond to the orientations of the two experimental curves in Fig. 1 of ref. [14].

FIG. 13. Full simulations of the temperature and frequency dependent experimental data in Fig. 2 with the magnetic field applied approximately parallel to the hard four-fold axis of the crystal; the frequencies and temperatures are indicated in the figure. In order to obtain the best agreement, a slight 1° mis-alignment away from the hard plane was taken into account, i.e. $\theta = 89°$ and $\phi \sim 0°$. Indeed, the relative intensities of the α and β resonances are extremely sensitive to the angle θ. This is easily understood upon inspection of Fig. 1a, where it is seen that the relative energy separations of the lowest lying states are extremely sensitive to the field orientation. Therefore, the corresponding transition probabilities, which

depend on the differences between Boltzmann factors, will also depend very sensitively on the angle θ.

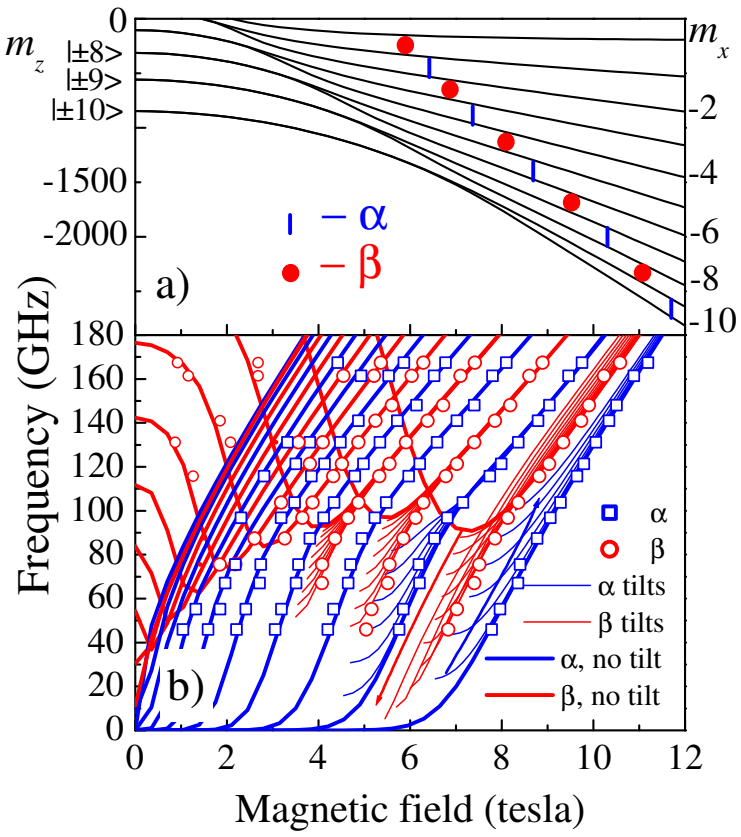

FIG. 1: S. Hill *et al.*

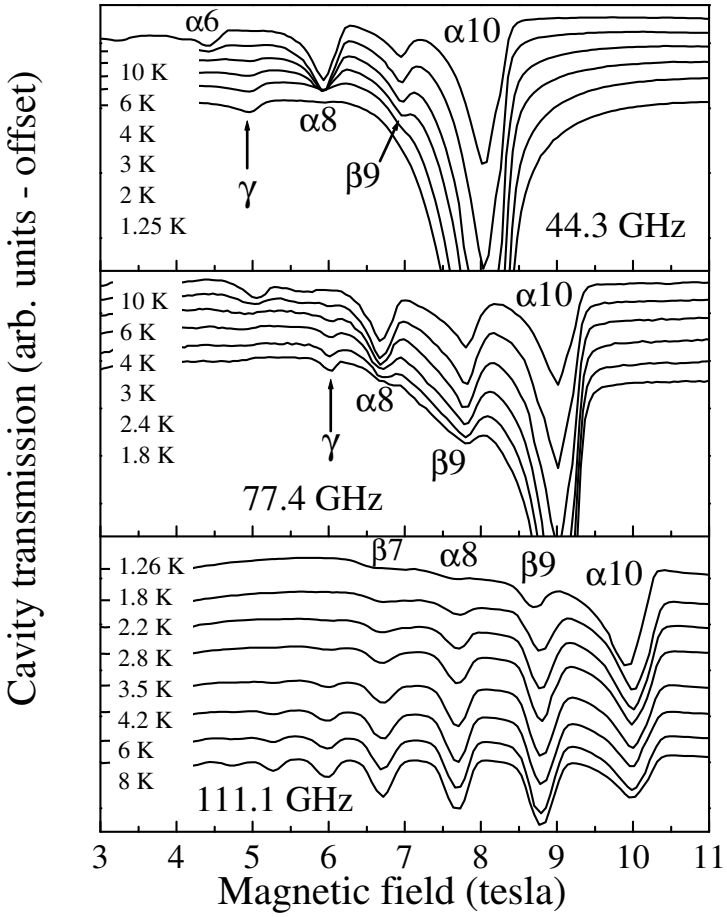

FIG. 2: S. Hill *et al.*

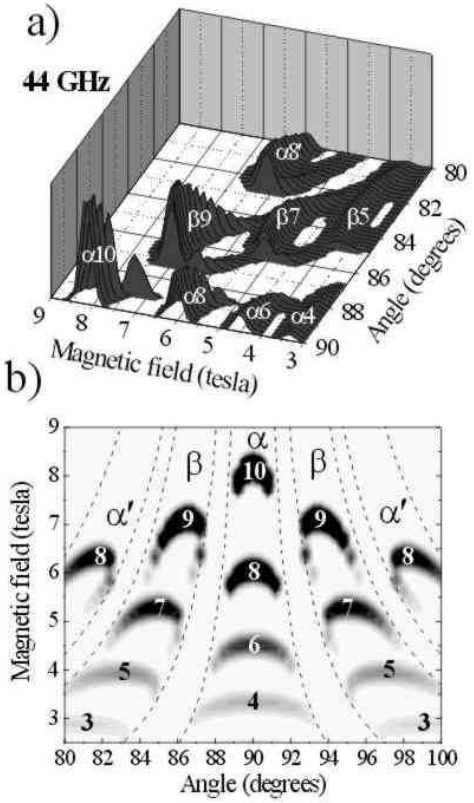

FIG. 3: S. Hill *et al.*

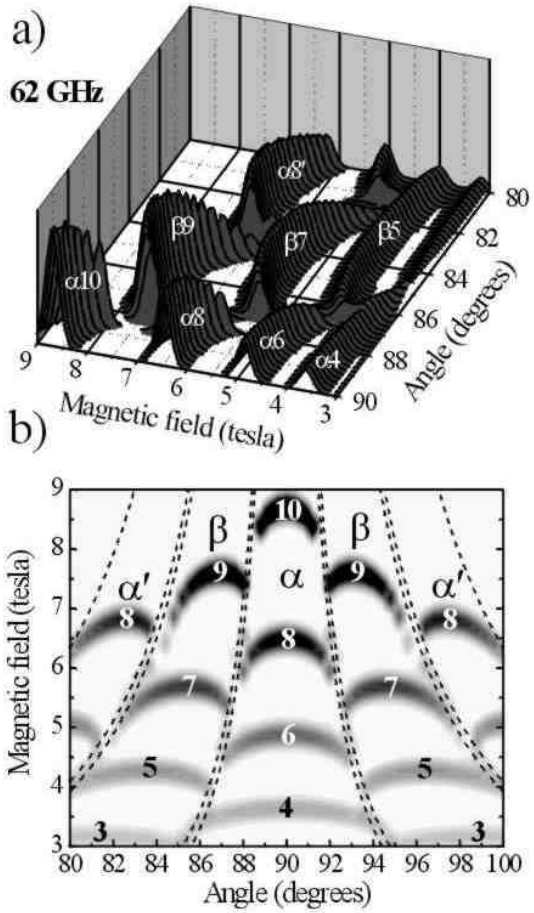

FIG. 4: S. Hill *et al.*

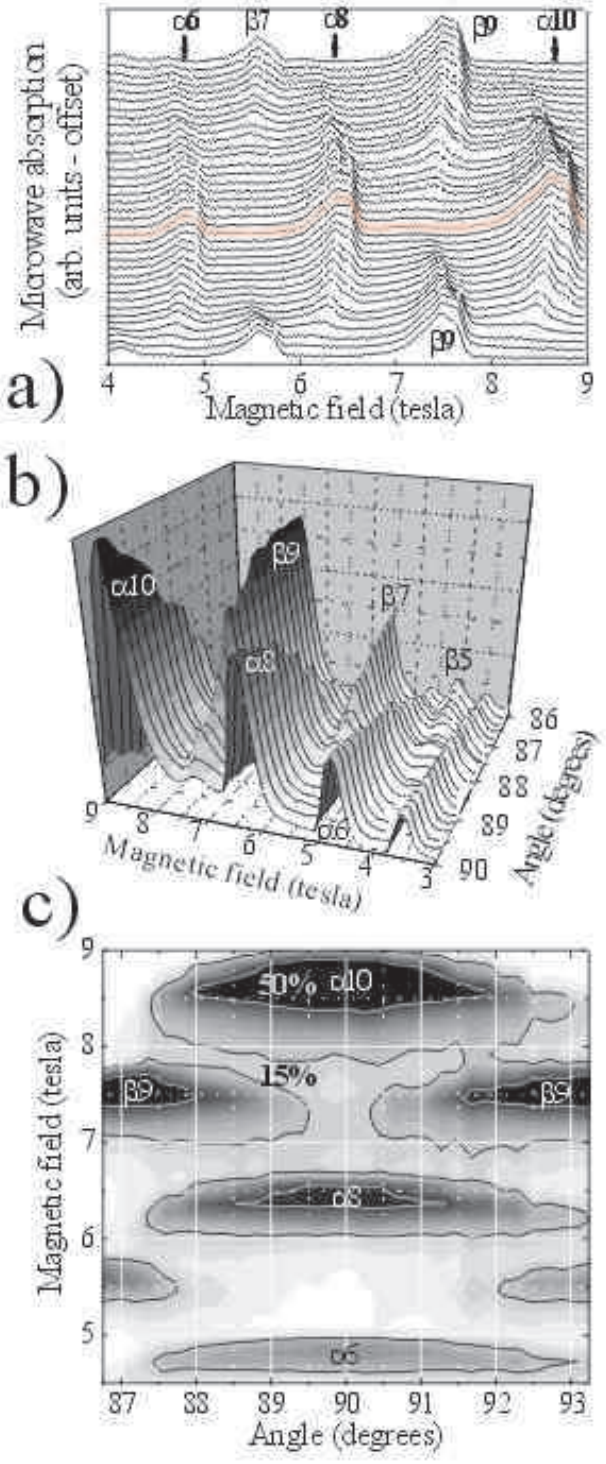

FIG. 5: S. Hill *et al.*

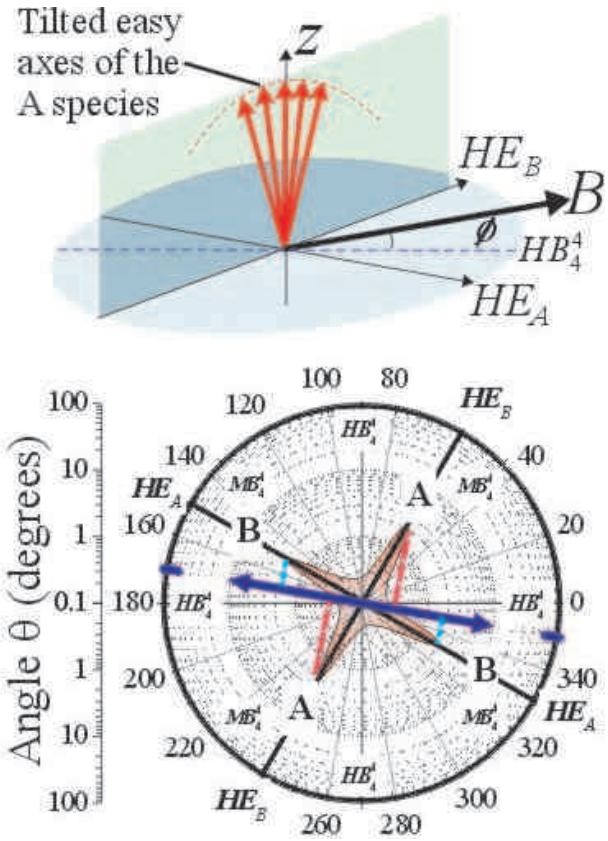

FIG. 6: S. Hill *et al.*

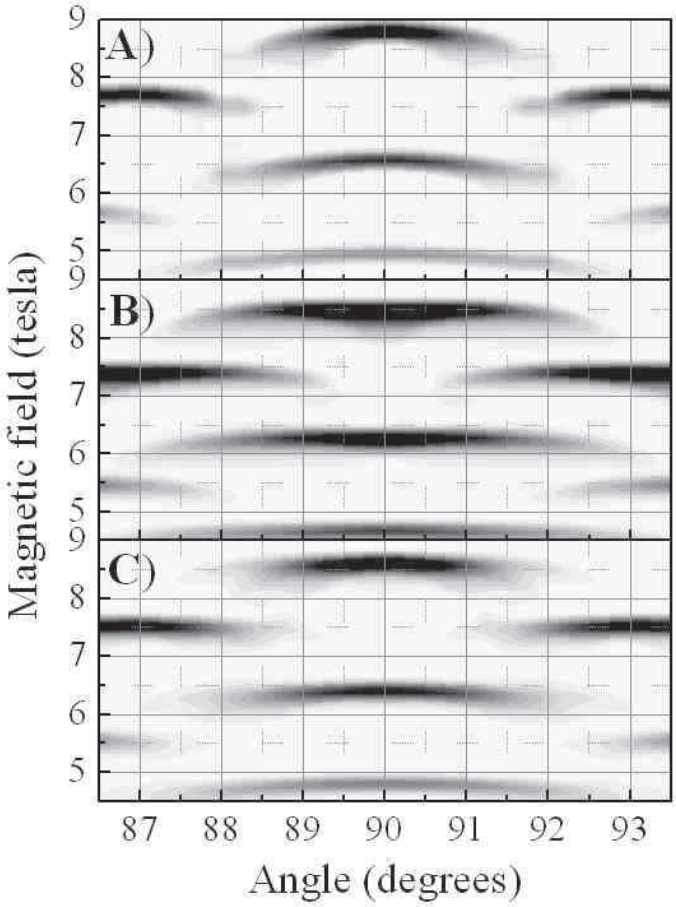

FIG. 7: S. Hill *et al.*

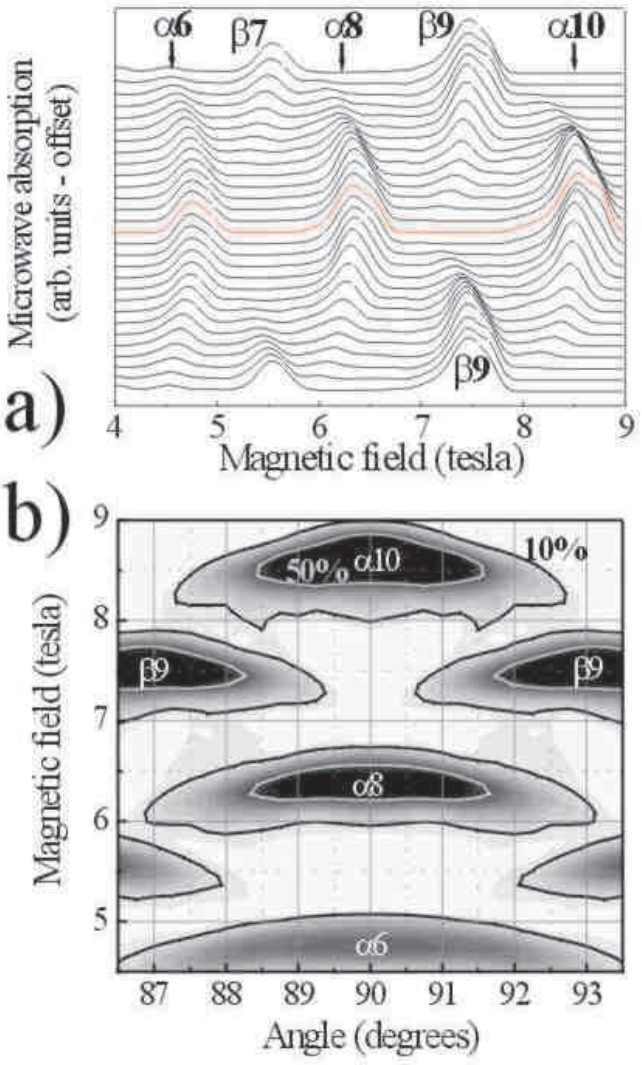

FIG. 8: S. Hill *et al.*

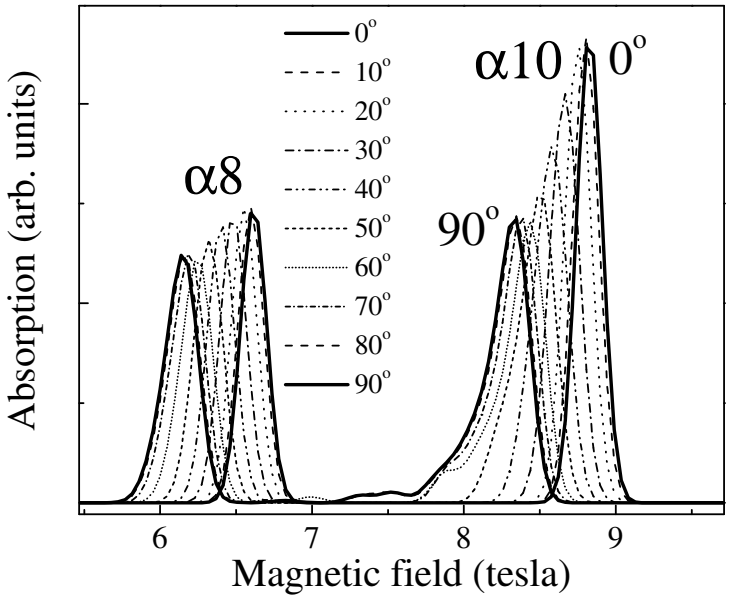

FIG. 9: S. Hill *et al.*

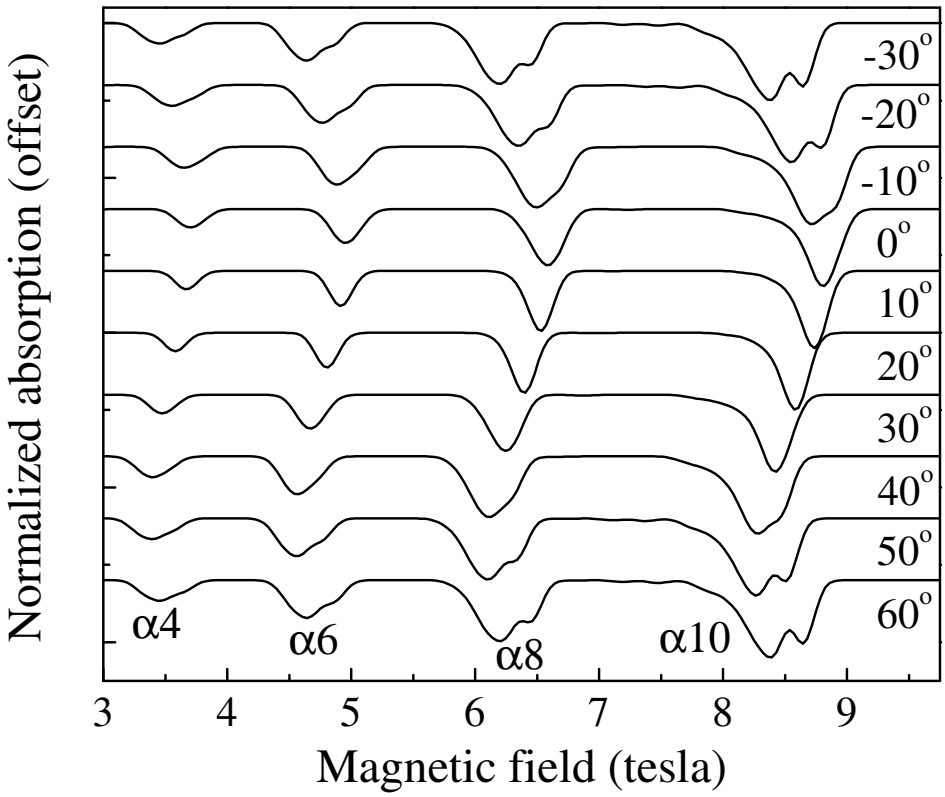

FIG. 10: S. Hill *et al.*

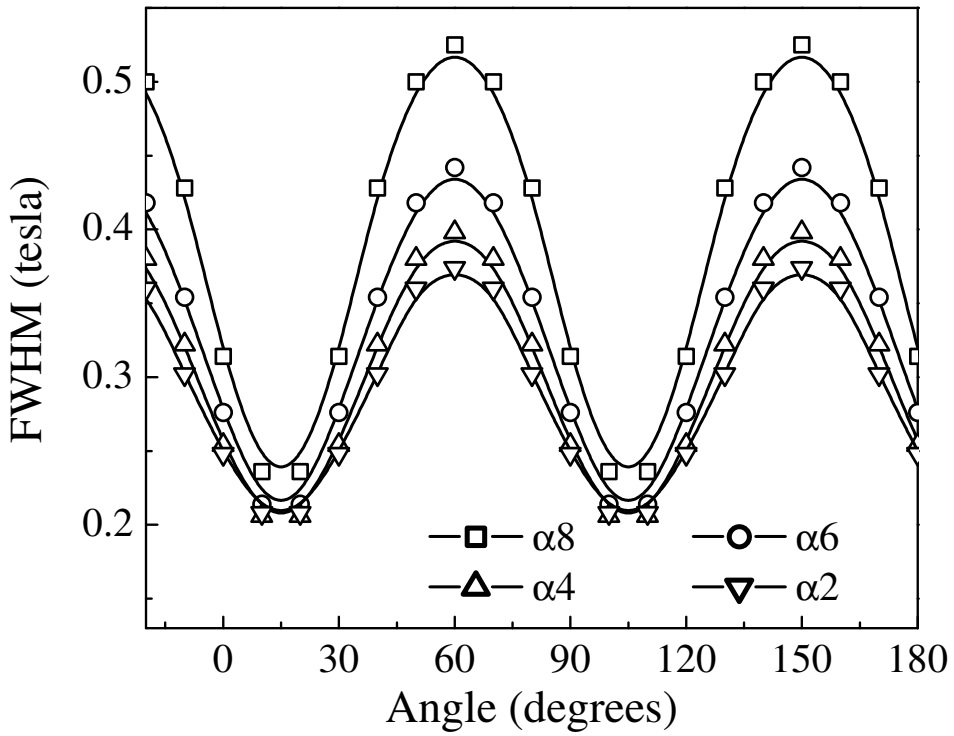

FIG. 11: S. Hill *et al.*

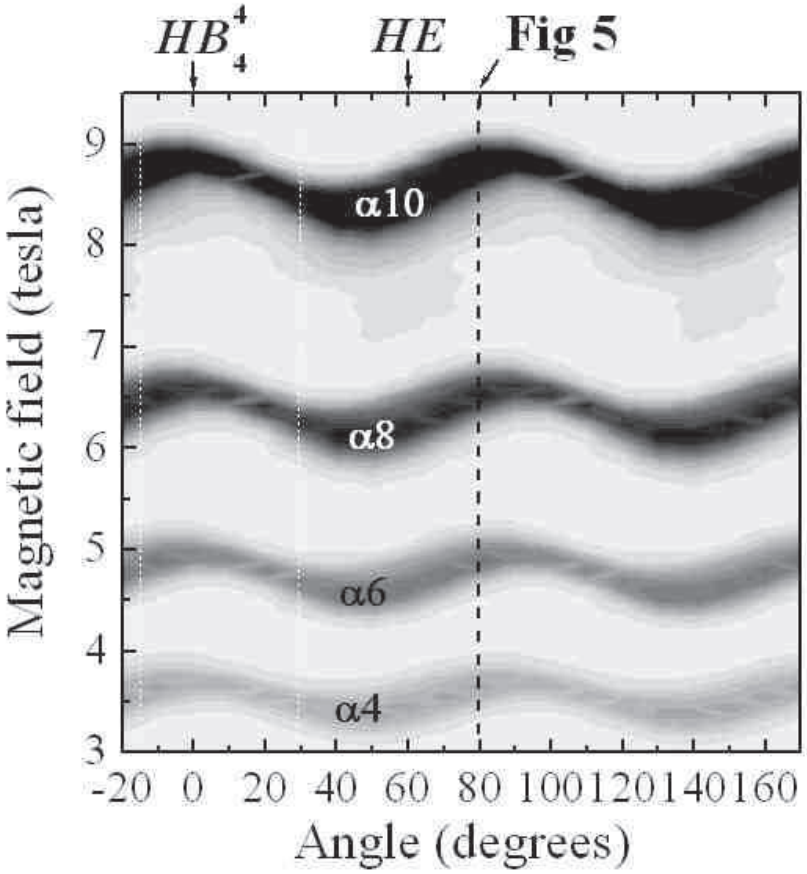

FIG. 12: S. Hill *et al.*

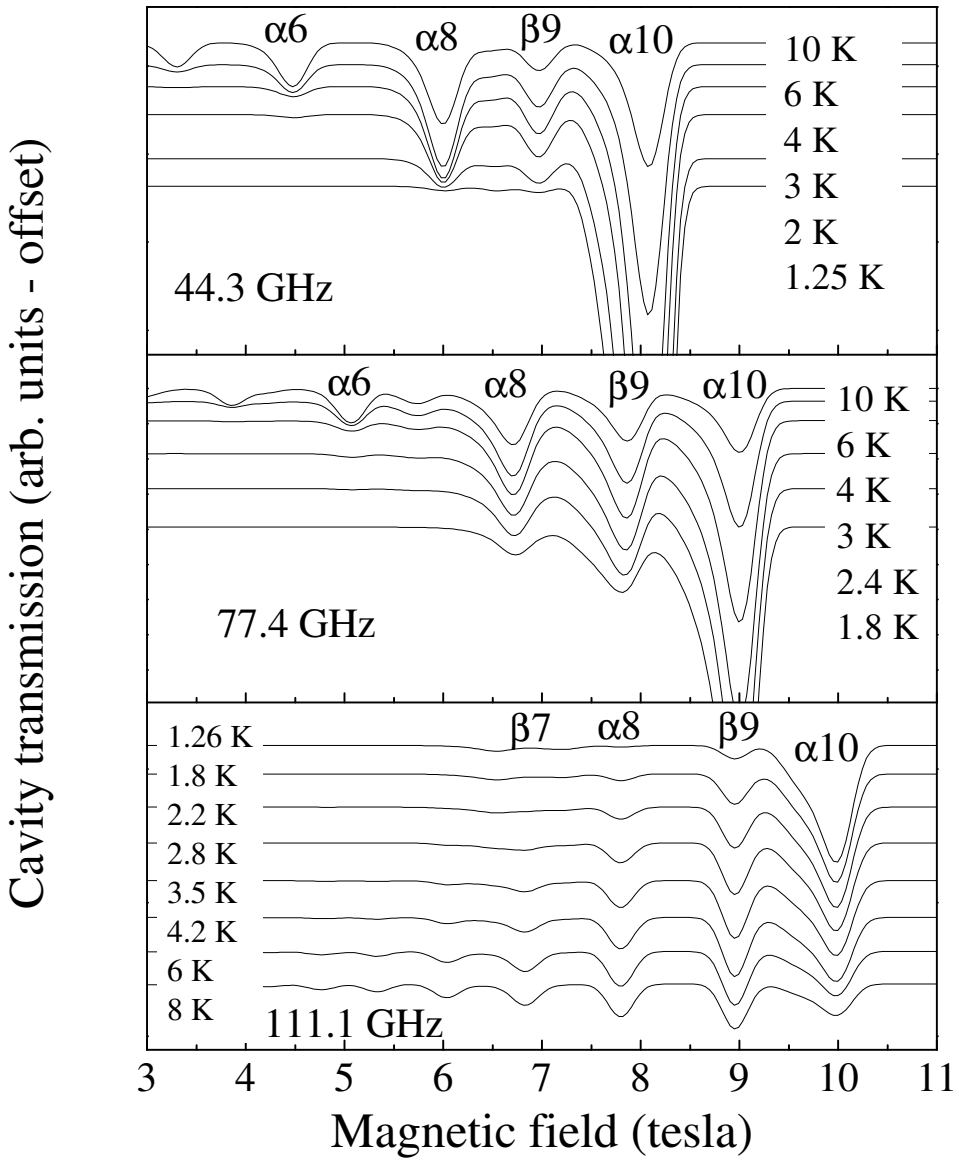

FIG. 13: S. Hill *et al.*